Frequency-Dependent Analysis of a Shielded Microstrip Step Discontinuity Using an Efficient Mode-Matching Technique

NIKOLAOS K. UZUNOGLU, MEMBER, IEEE, CHRISTOS N. CAPSALIS, AND CONSTANTINOS P. CHRONOPOULOS

Abstract—**The frequency-dependent characteristics of microstrip step discontinuities are analyzed by employing a mode-matching technique. The fields on both sides of a discontinuity are expanded in terms of the normal hybrid modes of the shielded microstrip line. The properties of these hybrid modes are determined by applying a previously developed analytical approach using singular integral equation techniques. In addition to propagating modes, higher order modes are also taken into account. The higher order modes are evanescent-type waves. The propagation constants of the evanescent waves in general are found to be complex numbers. A mode-matching procedure is developed to determine the reflection and transmission coefficients of the discontinuity. The use of two types of products to treat the boundary conditions for the continuity of the tangential electric and magnetic fields results in a highly efficient and numerically stable solution. Numerical results are computed for several step discontinuities and the results are compared with previously published data.**

I. INTRODUCTION

A COMMONLY encountered discontinuity structure in microstrip lines is the abrupt change of strip line width. This type of discontinuity is widely employed in low-pass filters, multisection quarter-wavelength transformers, stepped coupled line directional couplers, and many other microwave circuits. Therefore it is important to develop analytical techniques to compute accurately the characteristics of step discontinuities. These solutions can be incorporated into computer-aided design software packages of conventional and monolithic microwave integrated circuits. Furthermore, solutions developed for step discontinuity can serve as a starting point for more general treatments of discontinuity structures in planar microwave and millimeter-wave networks.

Several approaches have been proposed to treat the step discontinuities in microstrip lines. Presently there are several comprehensive reviews on this matter, such as the books by Hoffmann [1], Gupta *et al.* [2], [3], Edwards [4], and Mehran [5]. There is also a detailed revised description and a presentation of a rigorous frequency-dependent technique by Koster and Jansen [6].

A discrete element T-type two-port network consisting of two series inductive elements and a single shunt capacitive element has been proposed to model the step discontinuity approximately [7], [8]. Another approximate technique used by several authors is to treat the microstrip lines on both sides of the discontinuity with an equivalent magnetic waveguide model [9], [10]. Then the rather simple normal modes of the equivalent microstrip line are employed in formulating a mode-matching procedure. A system comprising an infinite set of equations involving the unknown expansion coefficients is obtained. This system could be solved numerically, by analytic matrix inversion, or by applying residue calculus techniques. The inherent limitations of these approximations and the necessity of seeking rigorous solutions have been discussed recently by Koster and Jansen [6]. The rigorous frequency-dependent method developed by Jansen [11], [12] to analyze step discontinuities, microstrip, and slot end effects is based on a spectral-domain approach using hybrid-mode analysis. The boundary value problem is reduced to the planar structure surface by incorporating initially into the field solutions the boundary conditions on the shielding walls. Then a Galerkin approach in conjunction with a spectral-domain Green's function interpolation technique with especially suited expansion functions is employed to solve the problem [11].

In this paper the very basic concepts of the mode-matching technique are employed to formulate the boundary condition problem associated with the microstrip step discontinuity problem. The fields on both sides of the discontinuity are expanded in terms of hybrid modes. The characteristics of these modes are determined by utilizing the analysis developed by Mittra and Itoh [13] in determining the dispersion characteristics of microstrip lines. The highly analytical approach used in computing the mode properties allows the development of an efficient mode-matching procedure. Furthermore, a fast convergence with number of modes is obtained by using products involving both microstrip line orthogonal mode functions. This feature is the key point of the proposed technique and is in agreement with the conclusions of Chu, Itoh, and Shih [14] in solving the step discontinuity problem using a magnetic wall equivalent waveguide microstrip model. The method presented in this paper seems to have some resemblance to techniques developed by Schmidt [15] and Chang [16], although the modal characteristics are determined by an entirely different method and the mode-matching technique used is completely different.

Manuscript received July 15, 1987; revised January 22, 1988.

The authors are with the Department of Electrical Engineering, National Technical University of Athens, Athens 10682, Greece.

IEEE Log Number 8821071.

0018-9480/88/0600-0976$01.00 ©1988 IEEE

The necessity of computing exactly the spectrum of higher order modes of microstrip lines leads us to the determination of evanescent waves with complex propagation constants having properties similar to those observed in finlines, as recently reported by Omar and Schünemann [19]. To the authors' knowledge, this is the first report of complex propagation constant waves in shielded microstrip lines.

In the following analysis the time dependence of field quantities is assumed to be $\exp(+j\omega t)$ and is suppressed throughout the analysis. The free-space propagation constant is shown with $k_0 = \omega/c$ where $c \cong 3\times10^8$ m/s is the velocity of electromagnetic waves in vacuum.

II. Formulation of the Boundary Value Problem

A. Computation of Mode Characteristics of Microstrip

The geometry pertaining to the microstrip discontinuity is given in Fig. 1, where the step discontinuity is located at the $z=0$ plane. The shielding box height and width are denoted by h and $(2L)$, respectively. The substrate dielectric constant and thickness are denoted by ϵ_r and d, respectively.

It is well known that microstrip line supports a dominant mode whose characteristics at sufficiently low frequencies can be determined by employing quasi-static TEM mode analysis. However, because of the partial dielectric filling, only hybrid modes can be guided. In characterizing microstrip lines the primary quantity to be known is the dominant mode propagation constant. Because of this, the literature on microstrip lines mostly concerns the computation of propagation constants with either quasi-static or frequency-dependent characteristics. There have been only few reports on the properties of higher order modes [17], [18]. The basic approach employed in the present analysis is to use the analytical technique developed by Mittra and Itoh [13] to determine the properties of higher order modes. In the following, the same notation as in [13] is adopted.

The mode characteristics are determined by computing the nontrivial solutions of the system [13],

$$\sum_{m=1}^{+\infty}\left(\hat{k}_p\delta_{pm}\alpha_m D_{pm}M_m k_p\right)\bar{A}_m^{(e)} - \sum_{n=1}^{+\infty}\left(b_n D_{pn}N_n K_p\right)\bar{A}_n^{(h)} = 0, \qquad p=1,2\cdots \quad (1)$$

$$\sum_{m=1}^{\infty}\left(-C_m D_{qm} - X_m K_q\right)\bar{A}_m^{(e)} + \sum_{n=1}^{\infty}\left(\hat{K}_q\delta_{qn} - d_n D_{qn} - Y_n K_q\right)\bar{A}_n^{(h)} = 0, \quad q=1,2\cdots \quad (2)$$

where $\hat{k}_p \equiv (2n-1)\pi/(2L)$, δ_{pm} is the Kronecker symbol, and $\bar{A}_m^{(e)}$, $\bar{A}_n^{(h)}$ are the normalized mode expansion coefficients [13, eqs. (12) and (13)]. The definitions of the α_m, b_m, c_m, d_m, M_m, N_m, X_m, and Y_m terms are given in [13, eqs. (22), (23), (24), (25), (48), (49), (52), and (53) respectively]. Furthermore, in order to compute the D_{nm}, P_{mq}, and K_n terms up to an arbitrary order of solution, new algorithms have been developed while in [13] only first-order results are presented. In the Appendix details of the procedures used in computing the values of D_{nm}, P_{mq}, and K_n are presented.

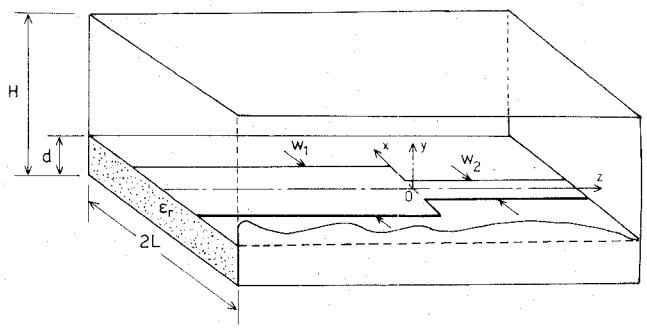

Fig. 1. Microstrip step discontinuity geometry.

The mode propagation constants β (which in general can take complex values) and their associated mode expansion coefficients $\bar{A}_m(e)$ and $\bar{A}_n^{(h)}$ are computed numerically by truncating the infinite system of (1) and (2) into a finite order system. To this end, it has been demonstrated by Mittra and Itoh [13] that the system in (1), (2) possesses highly convergent properties in terms of the truncation order. This is especially valid when only the value of the propagation constant is desired. It has been shown that taking only the first-order terms (i.e., terms with $m=1$ and $n=1$) and solving a 2×2 system, fairly good accuracy is obtained [13]. Assuming the numerical values of the β propagation constants that give a zero determinant for the system comprising (1) and (2) are known, the corresponding $\bar{A}_m^{(e)}$ and $\bar{A}_n^{(h)}$ coefficients can be determined by arbitrarily setting $\bar{A}_1^{(e)}=1$. Then the mode field distribution can be determined by first computing the potential functions,

$$\psi^{(e)} = \sum_{n=1}^{\infty}\cos\left(\hat{k}_n x\right)\begin{cases}\bar{A}_n^{(e)}\dfrac{\sinh\left(\alpha_n^{(1)}y\right)}{\sinh\left(\alpha_n^{(1)}d\right)} & \text{for } 0<y<d\\ \bar{B}_n^{(e)}\dfrac{\sinh\left(\alpha_n^{(2)}(h-y)\right)}{\sinh\left(\alpha_n^{(2)}(h-d)\right)} & \text{for } d<y<h\end{cases} \quad (3)$$

$$\psi^{(h)} = \sum_{n=1}^{+\infty}\sin\left(\hat{k}_n x\right)\begin{cases}\bar{A}_n^{(h)}\dfrac{\beta\hat{k}_n}{\omega\mu_0}\dfrac{\cosh\left(\alpha_n^{(1)}y\right)}{\alpha_n^{(1)}\sinh\left(\alpha_n^{(1)}d\right)} & \text{for } 0<y<d\\ \bar{B}_n^{(h)}\dfrac{\cosh\left(\alpha_n^{(2)}(h-y)\right)}{\sinh\left(\alpha_n^{(2)}(h-d)\right)} & \text{for } d<y<h\end{cases} \quad (4)$$

where

$$\bar{B}_n^{(e)} = \frac{\epsilon_r - \bar{\beta}^2}{1-\bar{\beta}^2}\bar{A}_n^{(e)}$$

$$\bar{B}_n^{(h)} = \frac{\beta\hat{k}_n}{\omega\mu_0}\frac{1}{\alpha_n^{(2)}}\left(\frac{1-\epsilon_r}{1-\bar{\beta}^2}\bar{A}_n^{(e)} - \bar{A}_n^{(h)}\right)$$

$$\bar{\beta} = \beta/k_0,\ \mu_0 = 4\pi\times 10^{-7}\ (\mathrm{H/m}).$$

Then the electric and the magnetic field for a specific mode with $\beta = \beta_m$ can be computed by using the relations

$$\boldsymbol{E}_m(\boldsymbol{r}) = \left(j\frac{k^2(y)-\beta_m^2}{\beta_m}\psi^{(e)}\hat{z} + \boldsymbol{e}_m(x,y)\right)e^{-j\beta_m z} \quad (5)$$

$$\boldsymbol{H}_m(\boldsymbol{r}) = \left(j\frac{k^2(y)-\beta_m^2}{\beta_m}\psi^{(h)}\hat{z} + \boldsymbol{h}_m(x,y)\right)e^{-j\beta_m z} \quad (6)$$

where

$$k(y) = k_0\sqrt{\epsilon(y)}$$

$$\epsilon(y) = \begin{cases}\epsilon_r & \text{for } 0 < y < d\\ 1 & \text{for } d < y < h\end{cases}$$

and the transversal field components are

$$\boldsymbol{e}_m(x,y) = \nabla_t\Psi^{(e)} - \frac{\omega\mu_0}{\beta_m}\hat{z}\times\nabla_t\Psi^{(h)} \quad (7)$$

$$\boldsymbol{h}_m(x,y) = \frac{\omega\epsilon(y)}{\beta_m}\hat{z}\times\nabla_t\Psi^{(e)} + \nabla_t\Psi^{(h)} \quad (8)$$

with

$$\nabla_t = \hat{x}\frac{\partial}{\partial x} + \hat{y}\frac{\partial}{\partial y}.$$

In (5)–(8) the subscript m indicates the mode number.

The microstrip line being an inhomogeneously dielectric loaded waveguide, the mode power orthogonality is satisfied [19]:

$$\int_A\int\left(\boldsymbol{e}_m(x,y)\times\boldsymbol{h}_{m'}^*(x,y)\right)\cdot\hat{z}\,dx\,dy = \delta_{mm'}C_m \quad (9)$$

where A is the cross-sectional area of the microstrip and the mode power coefficients C_m are computed by substituting (3), (4), (7), and (8) into (9) and performing the integrations for the x and y variables. The expression for the C_m coefficient is given in the Appendix.

The closed wall nature of the shielded microstrip line ensures the existence of only discrete eigenwaves, excluding the possibility of having a continuous spectrum of modes observed in open microstrip line. Then, the roots β_m of the determinant of the system comprising (1) and (2) should be determined carefully and the modes should be treated as an ordered set. In practice only a single mode is allowed to propagate on microstrip line. There are an infinite number of evanescent waves. Numerical computations showed that usually the evanescent waves have purely imaginary propagation constants and therefore they are strongly attenuated along the propagation axis. However, in some cases, it is possible to have complex β roots of the determinant of the system (1) and (2). These complex roots are traced by applying the procedure described in [19]. The properties of the complex microstrip modes will be discussed elsewhere. In Table I mode propagation constants of two sample cases are given at 10 GHz and 20 GHz.

TABLE I
NUMERICAL RESULTS FOR THE MODE PROPAGATION CONSTANTS AT 10 GHz AND 20 GHz

Frequency = 10 GHz

m	w = 0.953 mm β_m (mm^{-1})	w = 4.572 mm β_m (mm^{-1})
1	0.7884+j0.0	0.3021+j0.0
2	0.0-j0.2483	0.0-j0.2469
3	0.0-j0.5547	0.0-j0.5508
4	0.0-j0.5886	0.0-j0.6027
5	0.0-j0.9652	0.0 j0.9640
6	0.0-j1.0209	0.0-j0.9773
7	0.00449-j1.0849	0.0-j1.0731
8	-0.00449-j1.0849	0.0-j1.1023
9	0.0-j1.1075	0.0-j1.1236

Frequency = 20 GHz

m	w = 0.953 mm β_m (mm^{-1})	w = 4.572 mm β_m (mm^{-1})
1	0.5825+j0.0	0.6132+j0.0
2	0.2778+j0.0	0.2751+j0.0
3	0.0-j0.4127	0.0-j0.4034
4	0.0-j0.4558	0.0-j0.4802
5	0.0-j0.8880	0.0-j0.8626
6	0.0-j1.0450	0.0-j1.0631

$\epsilon_r = 2.32$, $L = 4.76$ mm, and $h = 6.35$ mm (see Fig. 1). The two microstrip widths are 0.953 mm and 4 572 mm.

In order to determine the numerical values of the β_m propagation constants in the first place, the simplified 2×2 version of (1) and (2) is solved. Then, the values of β_m and the expansion coefficients $\bar{A}_m^{(e)}$ and $\bar{A}_n^{(h)}$, ($\bar{A}_1^{(e)} = 1$) are determined accurately by using ($2M$) number of equations in the system (1), (2). To this end, a Regula–Falsi algorithm has been adopted to compute the roots of the determinant equation. In most cases only a single propagating ($\beta = \beta_1 = $ real) wave is encountered, although for sufficiently large ϵ_r and $k_0 d$ values a second propagating mode could exist.

The convergence patterns of the modal field expansion coefficients $A_n^{(e)}$ for a sample microstrip line are presented in Table II, where a very good numerical stability and convergence are observed. Notice that the low-order coefficients ($A_1^{(e)}$, $A_2^{(e)}$; see the Appendix for the definition of $A_n^{(e)}$) in the case of evanescent modes are very insensitive to the order of solution M.

B. Mode-Matching Technique

In order to determine the frequency-dependent characteristics of the step discontinuity, an incident propagat-

TABLE II
MODAL FIELD EXPANSION COEFFICIENT CONVERGENCE

M	1	2	3	4	5	6	7
$\beta(mm^{-1})$	0.3000+j0.0	0.3017+j0.0	0.3020+j0.0	0.3021+j0.0	0.3021+j0.0	0.3021+j0.0	0.3021+j0.0
$A_n(e)$	5.0223+j0.0	4.9958+j0.0	4.9910+j0.0	4.9905+j0.0	4.9902+j0.0	4.9902+j0.0	4.9901+j0.0
		-2.7243+j0.0	-2.6457+j0.0	-2.6624+j0.0	-2.6636+j0.0	-2.6647+j0.0	-2.6649+j0.0
			0.4844+j0.0	0.5160+j0.0	0.5202+j0.0	0.5214+j0.0	0.5218+j0.0
				0.2677+j0.0	0.2611+j0.0	0.2610+j0.0	0.2608+j0.0
					-0.1210+j0.0	-0.1220+j0.0	-0.1221+j0.0
						-0.0521+j0.0	-0.0517+j0.0
							0.0310+j0.0
$\beta(mm^{-1})$	0.0-j0.2470	0.0-j0.2469	0.0-j0.2469	0.0-j0.2469	0.0-j0.2469	0.0-j0.2469	0.0-j0.2469
$A_n(e)$	0.0-j6.8013	0.0-j6.8038	0.0-j6.8041	0.0-j6.8041	0.0-j6.8041	0.0-j6.8041	0.0-j6.8041
		-3.0447+j0.0	-3.0285+j0.0	-3.0329+j0.0	-3.0332+j0.0	-3.0334+j0.0	-3.0334+j0.0
			0.6759+j0.0	0.6828+j0.0	0.6836+j0.0	0.6838+j0.0	0.6838+j0.0
				0.1865+j0.0	0.1854+j0.0	0.1854+j0.0	0.1854+j0.0
					-0.1171+j0.0	-0.1172+j0.0	-0.1172+j0.0
						-0.0376+j0.0	-0.0375+j0.0
							0.0279+j0.0
$\beta(mm^{-1})$	0.0-j0.6020	0.0-j0.6026	0.0-j0.6027	0.0-j0.6027	0.0-j0.6027	0.0-j0.6027	0.0-j0.6027
$A_n(e)$	0.0-j2.7057	0.0-j2.7030	0.0-j2.7028	0.0-j2.7028	0.0-j2.7028	0.0-j2.7028	0.0-j2.7028
		-3.9191+j0.0	-3.8977+j0.0	-3.9019+j0.0	-3.9022+j0.0	-3.9021+j0.0	-3.9020+j0.0
			0.7390+j0.0	0.7444+j0.0	0.7449+j0.0	0.7448+j0.0	0.7447+j0.0
				0.1941+j0.0	0.1935+j0.0	0.1935+j0.0	0.1936+j0.0
					-0.1218+j0.0	-0.1218+j0.0	-0.1218+j0.0
						-0.0381+j0.0	-0.0382+j0.0
							0.0286+j0.0

$f = 10$ GHz, $\epsilon_r = 2.32$, $L = 4.76$ mm, $h = 6.35$ mm (see Fig. 1), and $w = 4.572$ mm.

ing wave ($\beta = \beta_1$) from $z = -\infty$ toward $z = 0$ (see Fig. 1) is taken. Furthermore, assuming the mode properties of the microstrips on both sides of the discontinuity are known, inside the $z < 0$ half-space the transversal electric and magnetic field components can be expressed as a superposition of the incident and the sum of all the reflected waves:

$$\boldsymbol{E}_t(x, y, z) = \boldsymbol{e}_1(x, y)e^{-j\beta_1 z} + \sum_{n=1}^{+\infty} A_n \boldsymbol{e}_n(x, y)e^{+j\beta_n z} \quad (10)$$

$$\boldsymbol{H}_t(x, y, z) = \boldsymbol{h}_1(x, y)e^{-j\beta_1 z} - \sum_{n=1}^{+\infty} A_n \boldsymbol{h}_n(x, y)e^{+j\beta_n z} \quad (z < 0) \quad (11)$$

where A_n ($n = 1, 2, \cdots$) are unknown coefficients to be determined. The corresponding transversal field components inside the $z > 0$ semi-infinite space can be written as follows:

$$\boldsymbol{E}_t'(x, y, z) = \sum_{m=1}^{+\infty} B_m \boldsymbol{e}_m'(x, y)e^{-j\beta_m' z} \quad (12)$$

$$\boldsymbol{H}_t'(x, y, z) = \sum_{m=1}^{+\infty} B_m \boldsymbol{h}_m'(x, y)e^{-j\beta_m' z} \quad (z > 0) \quad (13)$$

where the prime symbol is used to distinguish the two different microstrip line modal field distributions and propagation constants. Again B_m ($m = 1, 2, \cdots$) are unknown coefficients to be determined.

Applying the boundary conditions on the $z = 0$ plane for the continuity of the transversal field components,

$$\boldsymbol{e}_1(x, y) + \sum_{n=1}^{+\infty} A_n \boldsymbol{e}_n(x, y) = \sum_{m=1}^{+\infty} B_m \boldsymbol{e}_m'(x, y) \quad (14)$$

$$\boldsymbol{h}_1(x, y) - \sum_{n=1}^{+\infty} A_n \boldsymbol{h}_n(x, y) = \sum_{m=1}^{+\infty} B_m \boldsymbol{h}_m'(x, y) \quad (z = 0) \quad (15)$$

are obtained. Then, in order to determine the unknown A_n and B_n expansion coefficients, (12) and (13) should be transformed by some means into an infinite system of equations and the dependence on the x and y coordinates should be removed. To this end, it is possible to pursue several strategies in computing the A_n and B_n coefficients. A quite similar problem of choosing the best mode-matching approach when the magnetic wall microstrip model is employed has been addressed recently by Chu, Itoh, and Shih [14]. Furthermore, the trial of several approaches showed that there is also an optimal strategy in terms of convergence behavior in the present hybrid mode analysis. To this end it is found that the optimal way of solving (14) and (15) is to take the vector products of them with $\boldsymbol{e}_m(x, y)$ and $\boldsymbol{h}_m'(x, y)$, respectively. Following the orthogonality properties of the $\boldsymbol{e}_m, \boldsymbol{h}_m$ and $\boldsymbol{e}_m', \boldsymbol{h}_m'$ eigenwaves

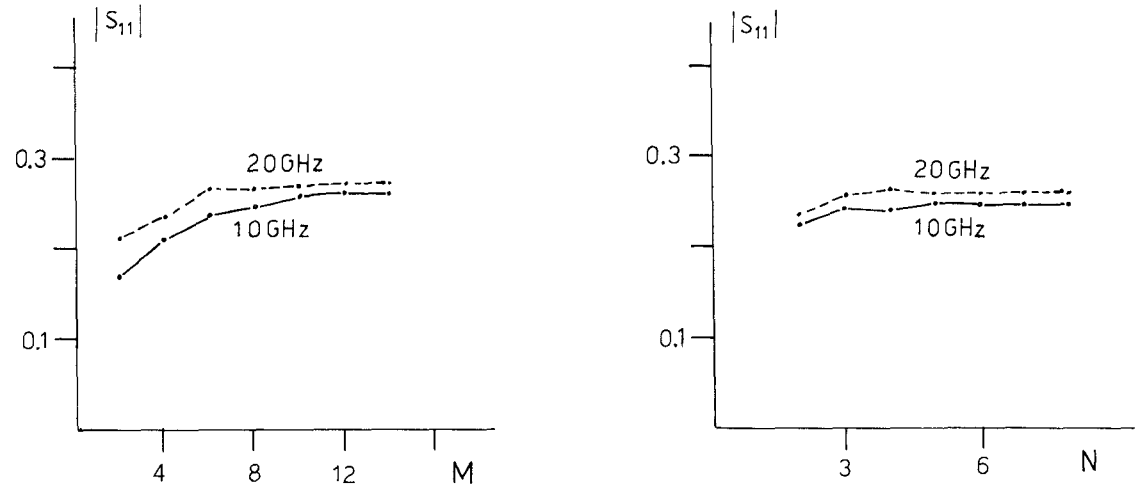

Fig. 2. Convergence of $|S_{11}|$ reflection coefficient with M (truncation order of (1) and (2)) and N (number of modes) taken into account on both sides of discontinuity for $w_2/w_1 = 2$, $w_1/d = 3$, and $\epsilon_r = 2.32$.

given in (9), it is found that

$$C_1\delta_{n1} + A_nC_n = \sum_{m=1}^{+\infty} B_mC_{mn} \tag{16}$$

$$C_{m1}^* - \sum_{n=1}^{+\infty} A_nC_{mn}^* = B_mC_m^{*\prime} \tag{17}$$

where

$$C_{mn} = \int_A\int (\boldsymbol{e}_m'(x,y)\times \boldsymbol{h}_n^*(x,y))\,dx\,dy \tag{18}$$

are coupling integrals and C_n, C_n' have already been defined in (9).

Eliminating the B_m coefficient in (16) and (17), a new set of infinite system of equations is obtained:

$$A_nC_n + \sum_{k=1}^{\infty} A_k\left(\sum_{m=1}^{\infty}\frac{C_{mn}C_{mk}^*}{C_m^{*\prime}}\right) = \left(\sum_{m=1}^{\infty} C_{mn}\frac{C_{m1}^*}{C_m^{*\prime}} - C_1\delta_{n1}\right), \quad n=1,2,3,\cdots \tag{19}$$

This system constitutes the basis of the analytical approach of this paper. In order to determine the unknown expansion coefficients $A_1, A_2, \cdots$, the infinite summations appearing in (19) should be truncated into finite order by taking N terms (modes). Then, convergence of the computed results is examined to verify the accuracy. This subject will be treated in the next section.

The coupling integrals C_{mn} are computed by substituting the field expressions given in (7) and (8) into (18) and then performing the integrations for the x and y variables. The result of this analysis is given in the Appendix. After determining the A_n reflected wave coefficients, the transmitted wave expansion coefficients B_n are computed easily by using (17), where of course, the same Nth-order truncation of the infinite sums is used. In practice the interested quantities are the dominant mode reflection S_{11} and transmission S_{21} coefficients. Then $S_{11} = A_1$ and according to the definition of S parameters

$$S_{21} = B_1\sqrt{\frac{C_1'}{C_1}}. \tag{20}$$

III. Numerical Results

Numerical computations have been performed by applying the theory developed in Section II. For each pair of microstrip lines the spectrum of propagation and evanescent waves is determined up to sufficient order by taking $2M$ equations in the system (1), (2). A perfect agreement with the β values given in [13] is observed. Then, (19) is solved numerically by keeping N terms in the infinite summation. Both M and N truncations affect the accuracy of the obtained results for the S_{11} and S_{21} parameters. In each case, extensive convergence tests have been performed to verify the accuracy of the obtained results. In Figs. 2 and 3 sample convergence patterns are presented. In general, the phase quantities $\angle S_{11}$ and $\angle S_{21}$ are much more sensitive than the corresponding amplitudes $|S_{11}|$ and $|S_{21}|$. The truncation order M of the system of (1), (2) seems to have the primary role in the convergence. The numerical results presented in this paper have been computed by using $M = 8$ and $N = 8$ truncations.

The "relative convergence" aspect [20] by taking a nonequal number of modes in (19) in the two microstrip lines has been investigated. It has been shown that some improvement in the convergence speed can be achieved by taking the ratio of mode numbers equal to the ratio of microstrip widths. However, because of the smooth convergence of the results presented in this paper no use is made of this property.

Several independent checks have been performed numerically, such as the validity of the power conservation, reciprocity ($S_{21} = S_{12}$), and the boundary conditions on the $y = d$ plane (see Fig. 1) by the mode field distributions. Furthermore, the orthogonality conditions given in (9) have been verified by direct numerical computation.

Step discontinuities on low $\epsilon_r = 2.32$ (polyethylene) and high $\epsilon_r = 10$ (alumina) dielectric constant substrates have been considered. In all the computed results the shielding box dimensions are taken to be

$$2L = 0.53 \text{ mm} \qquad h = 6.35 \text{ mm}.$$

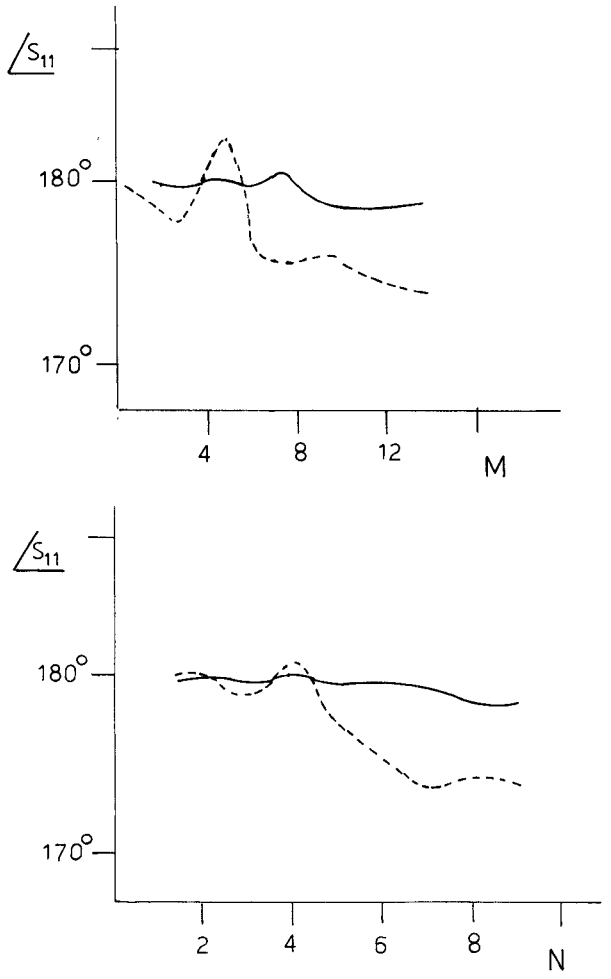

Fig. 3. Convergence of $\angle S_{11}$ with M and N truncation orders for the same discontinuity of Fig. 2.

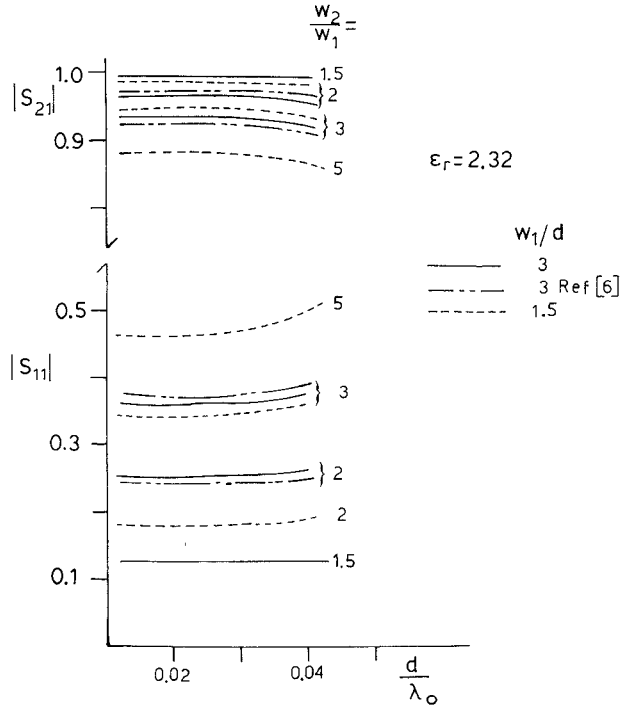

Fig. 4. Variation of $|S_{11}|$ and $|S_{21}|$ parameters with d/λ_0 (λ_0 being the free-space wavelength) for several discontinuity dimensions and $\epsilon_r = 2.32$.

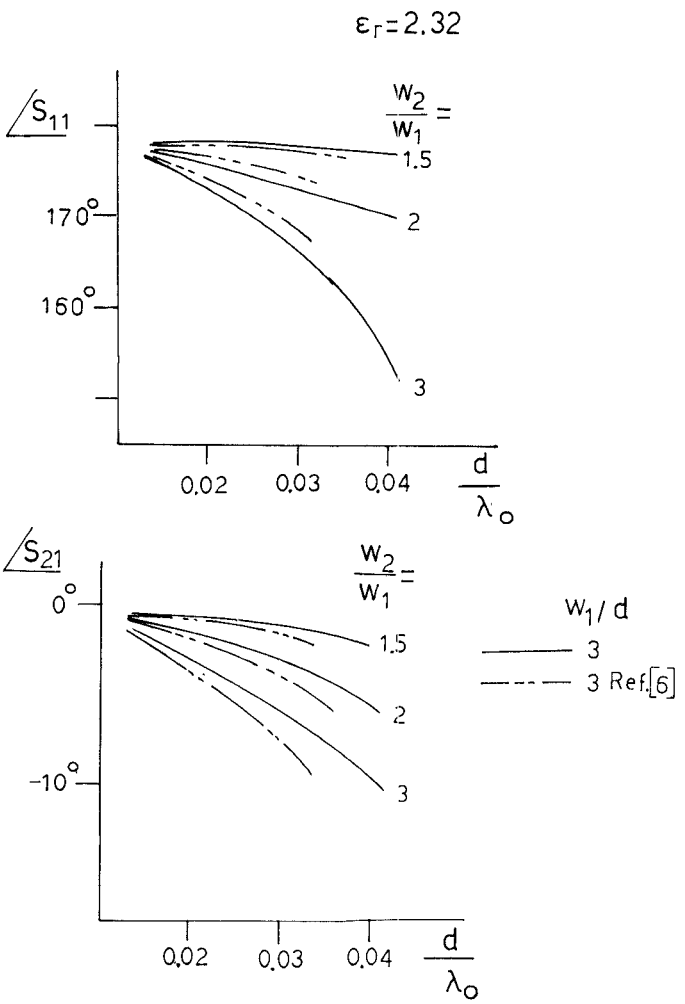

Fig. 5. Variation of $\angle S_{11}$ and $\angle S_{21}$ phase parameters with d/λ_0 for several discontinuity dimensions and $\epsilon_r = 2.32$.

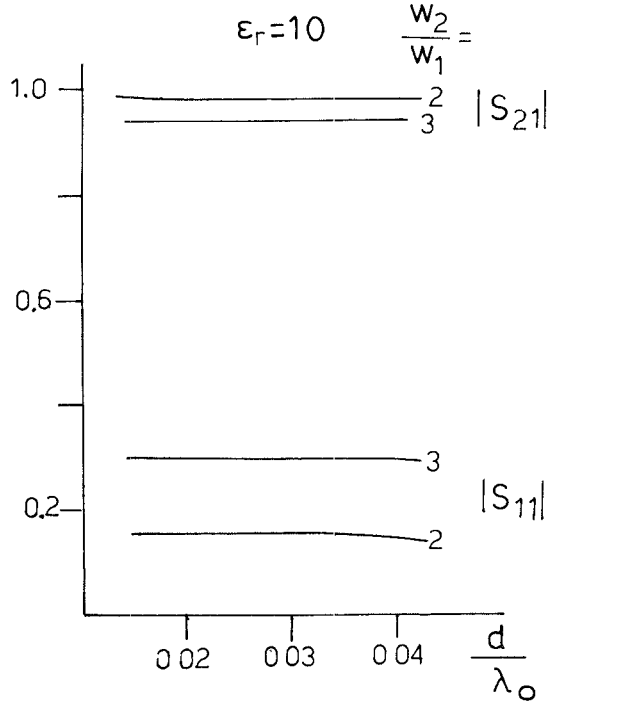

Fig. 6. Variation of $|S_{11}|$ and $|S_{21}|$ parameters with d/λ_0 for several discontinuity dimensions, $\epsilon_r = 10$, and $w_1/d = 1.5$.

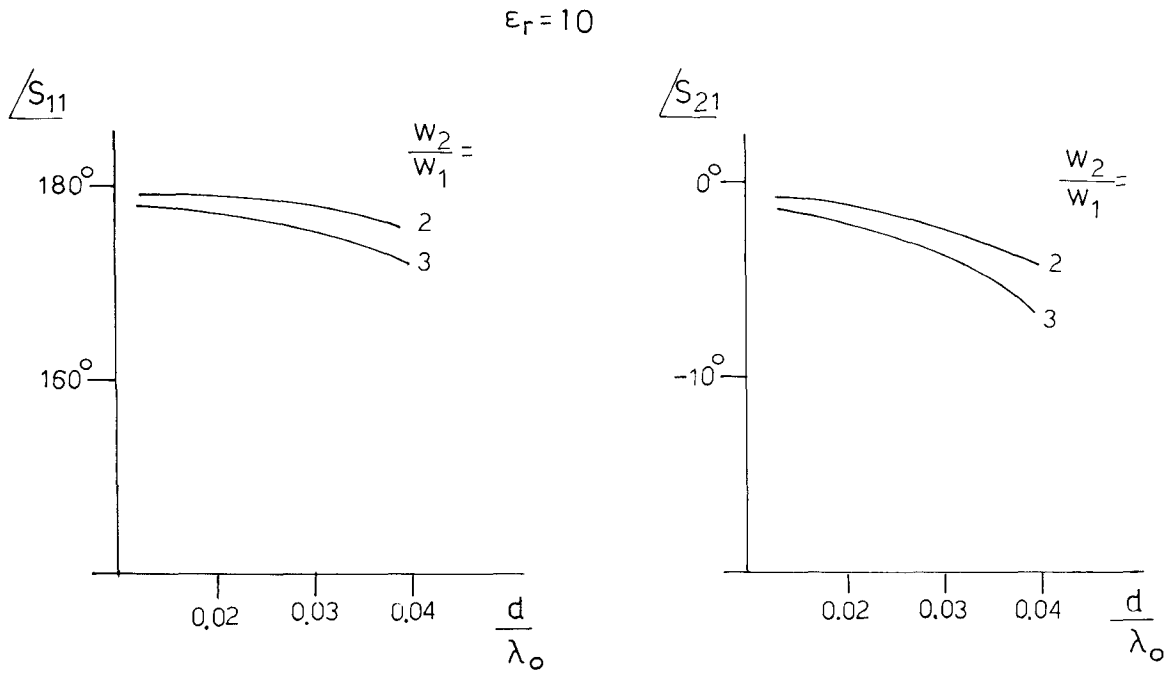

Fig. 7. Variation of $\angle S_{11}$ and $\angle S_{21}$ phase parameters with d/λ_0 for several discontinuity dimensions, $\epsilon_r = 10$, and $w_1/d = 1.5$.

The scattering parameters S_{11} and S_{21} are presented in terms of their amplitudes and phases versus the normalized substrate thickness d/λ_0, where λ_0 is the free-space wavelength ($\lambda_0 = 2\pi/k_0$).

In Figs. 4 and 5 results are given for the $\epsilon_r = 2.32$ substrate, several microstrip width w_1/w_2 ratios, where w_1 and w_2 are defined in Fig. 1, and two w_1/d ratios. The results obtained are compared with those given by Koster and Jansen [6], which are also drawn on the same figures for $w_1/d = 3$ and $w_1/w_2 = 2$ and 3. Good agreement is observed for the $|S_{11}|$, $|S_{21}|$ amplitude quantities, while the comparison of $\angle S_{11}$ and $\angle S_{21}$ phase quantities is also reasonably good.

Discontinuities in microstrip lines with $\epsilon_r = 10$ alumina substrate have been computed and are presented in Figs. 6 and 7. A similar behavior is observed with the $\epsilon_r = 2.32$ substrate case.

IV. Conclusions

A frequency-dependent analysis has been presented for the microstrip discontinuity problem. The proposed method is shown to be efficient in terms of the required numerical labor and is easy to program. The evanescent mode spectrum of microstrip lines has been investigated and the existence of modes with complex propagation constants has been verified. Numerical results have been presented for several discontinuity structures and a comparison with previously published data has been performed. In principle the same method could be used to treat other types of discontinuity problems in microstrip lines and the junctions between different types of waveguides and microstrip lines.

Appendix

A. Computation of P_{mq}, D_{nm} and K_n Terms

Following a standard trigonometric analysis, the P_{mq} terms defined in [13, eq. (68)] after algebraic manipulations, are found to be

$$P_{mq} = \begin{cases} \displaystyle\sum_{l=2v}^{m-1} B_{ml} \sum_{k=v}^{[l/2]} \binom{l}{2k} \alpha_2^{2k} \alpha_1^{l-2k} \frac{1}{2^{2k-1}} \binom{2k}{k-v}, & q = 2v \\ \displaystyle\sum_{l=2v-1}^{m-1} B_{ml} \sum_{k=v}^{[l+1/2]} \binom{l}{2k-1} \times \alpha_2^{2k-1} \alpha_1^{l-2k+1} \frac{1}{2^{2k-2}} \binom{2k-1}{k-v}, & q = 2v-1 \\ \displaystyle\sum_{l=0}^{m-1} B_{ml} \sum_{k=0}^{[l/2]} \binom{l}{2k} \alpha_2^{2k} \alpha_1^{l-2k} \frac{1}{2^{2k}} \binom{2k}{k}, & q = 0 \end{cases}$$

where α_1 and α_2 are defined in [13, eq. (61)] and the A_{nq} and B_{nq} are given by the recursive relations

$$\sum_{q=v}^{n-1} A_{nq} \binom{q}{v} = (2n-1) \frac{2^v}{(2v+1)!} \prod_{l=1}^{v} (n-l)(n+l-1), \qquad v \neq 0$$

$$\sum_{q=0}^{n-1} A_{nq} = 2n-1$$

$$\sum_{q=v}^{n-1} B_{nq} \binom{q}{v} = \frac{2^v}{(2v)!} \prod_{l=1}^{v} (n-l)(n+l-1), \qquad v \neq 0$$

$$\sum_{q=0}^{n-1} B_{nq} = 1.$$

Following an analogous procedure, the D_{nm} and K_n terms, defined in [13, eqs. (73) and (72) respectively], are given as follows:

$$D_{nm} = \frac{\alpha_2}{2} \sum_{q=1}^{m-1} P_{mq} \sum_{l=0}^{n-1} A_{nl} \sum_{k=0}^{l} \binom{l}{k} \alpha_2^k \alpha_1^{l-k} (X_{kq} - Y_{kq}) - \alpha_2 P_{m0} \sum_{q=1}^{n-1} A_{nq} \sum_{k=1}^{[q+1/2]} \binom{q}{2k-1} \cdot \alpha_2^{2k-1} \alpha_1^{q-2k+1} \frac{1}{2^{2k}} \binom{2k}{k}$$

where

$$X_{kq} = \begin{cases} \frac{1}{2^k} \binom{k}{\frac{k-q-1}{2}} & \text{when } k-q+1 = \text{even and } q-1 \leqq k \\ 0 & \text{elsewhere} \end{cases}$$

$$Y_{kq} = \begin{cases} \frac{1}{2^k} \binom{k}{\frac{k-q+1}{2}} & \text{when } k-q+1 = \text{even and } q+1 \leqq k \\ 0 & \text{elsewhere} \end{cases}$$

and

$$K_n = \alpha_2 \sum_{q=0}^{n-1} A_{nq} \sum_{v=0}^{[q/2]} \alpha_2^{2v} \alpha_1^{q-2v} \frac{1}{2^{2v}} \binom{2v}{v} \binom{q}{2v}.$$

B. Computation of the C_n Terms ($n = 1, 2, -$)

The coefficients C_n defined in (9) are given as follows:

$$C_n = L \cdot \sum_{k=1}^{\infty} \left(-A_k^{(e)} \hat{k}_k + \frac{\omega\mu}{\beta_n} A_k^{(h)} \alpha_k^{(1)} \right) \cdot \left(-\frac{\omega \epsilon_0 \epsilon_r}{\beta_n} A_k^{(e)} \hat{k}_k + A_k^{(h)} \alpha_k^{(1)} \right)^* \cdot I1 + \left(-A_k^{(e)} \alpha_k^{(1)} + \frac{\omega\mu}{\beta_n} A_k^{(h)} \hat{k}_k \right) \cdot \left(-\frac{\omega \epsilon_0 \epsilon_r}{\beta_n} A_k^{(e)} \alpha_k^{(1)} + A_k^{(h)} \hat{k}_k \right)^* \cdot I2 + \left(B_k^{(e)} \hat{k}_k + \frac{\omega\mu}{\beta_n} B_k^{(h)} \alpha_k^{(2)} \right) \cdot \left(\frac{\omega \epsilon_0}{\beta_n} B_k^{(e)} \hat{k}_k + B_k^{(h)} \alpha_k^{(2)} \right)^* \cdot I3 + \left(B_k^{(e)} \alpha_k^{(2)} + \frac{\omega\mu}{\beta_n} B_k^{(h)} \hat{k}_k \right) \cdot \left(\frac{\omega \epsilon_0}{\beta_n} B_k^{(e)} \alpha_k^{(2)} + B_k^{(h)} \hat{k}_k \right)^* \cdot I4$$

where

$$\alpha_k^{(1)} = \sqrt{\hat{k}_k^2 + \beta_n^2 - \epsilon_r k_0^2}$$

$$\alpha_k^{(2)} = \sqrt{\hat{k}_k^2 + \beta_n^2 - k_0^2}$$

$$A_n^{(e)} = \frac{\overline{A}_n^{(e)}}{\sinh(\alpha_n^{(1)} d)} \qquad A_n^{(h)} = \frac{\beta \hat{k}_n}{\omega \mu_0 \alpha_n^{(1)} \sinh(\alpha_n^{(1)} d)} \overline{A}_n^{(h)}$$

$$B_n^{(e)} = \frac{\overline{B}_n^{(e)}}{\sinh(\alpha_n^{(2)}(h-d))} \qquad B_n^{(h)} = \frac{\overline{B}_n^{(h)}}{\sinh(\alpha_n^{(2)}(h-d))}$$

and $I1, I2, I3, I4$ are the following integrals:

$$I1 = \int_0^d \sinh(\alpha_k^{(1)} y) \cdot (\sinh(\alpha_k^{(1)} y))^* \, dy$$

$$I2 = \int_0^d \cosh(\alpha_k^{(1)} y) \cdot (\cosh(\alpha_k^{(1)} y))^* \, dy$$

$$I3 = \int_d^h \sinh(\alpha_k^{(2)}(h-y)) \cdot (\sinh(\alpha_k^{(2)}(h-y)))^* \, dy$$

$$I4 = \int_d^h \cosh(\alpha_k^{(2)}(h-y)) \cdot (\cosh(\alpha_k^{(2)}(h-y)))^* \, dy.$$

C. Computation of the C_{mn} Terms ($m(n) = 1, 2, 3, \cdots$)

The coefficients C_{mn} defined in (18) are given as follows:

$$C_{mn} = L \cdot \sum_{k=1}^{8be} \left(-A_{km}^{(e)} \hat{k}_k + \frac{\omega\mu}{\beta_m} A_{km}^{(h)} \alpha_{km}^{(1)} \right) \cdot \left(-\frac{\omega \epsilon_0 \epsilon_r}{\beta_n} A_{kn}^{(e)} \hat{k}_k + A_{kn}^{(h)} \alpha_{kn}^{(1)} \right)^* \cdot I1 + \left(-A_{km}^{(e)} \alpha_{km}^{(1)} + \frac{\omega\mu}{\beta_m} A_{km}^{(h)} \hat{k}_k \right) \cdot \left(-\frac{\omega \epsilon_0 \epsilon_r}{\beta_n} A_{kn}^{(e)} \alpha_{kn}^{(1)} + A_{kn}^{(h)} \hat{k}_k \right)^* \cdot I2 + \left(B_{km}^{(e)} \hat{k}_k + \frac{\omega\mu}{\beta_m} B_{km}^{(h)} \alpha_{km}^{(2)} \right) \cdot \left(\frac{\omega \epsilon_0}{\beta_n} B_{kn}^{(e)} \hat{k}_k + B_{kn}^{(h)} \alpha_{kn}^{(2)} \right)^* \cdot I3 + \left(B_{km}^{(e)} \alpha_{km}^{(2)} + \frac{\omega\mu}{\beta_m} B_{km}^{(h)} \hat{k}_k \right) \cdot \left(\frac{\omega \epsilon_0}{\beta_n} B_{kn}^{(e)} \alpha_{kn}^{(2)} + B_{kn}^{(h)} \hat{k}_k \right)^* \cdot I4$$

where

$$\alpha_{km}^{(1)} = \sqrt{\hat{k}_k^2 + \beta_m^2 - \epsilon_r k_0^2} \qquad \alpha_{kn}^{(1)} = \sqrt{\hat{k}_k^2 + \beta_n^2 - \epsilon_r k_0^2}$$

$$\alpha_{km}^{(2)} = \sqrt{\hat{k}_k^2 + \beta_m^2 - k_0^2} \qquad \alpha_{kn}^{(2)} = \sqrt{\hat{k}_k^2 + \beta_n^2 - k_0^2}$$

and $I1, I2, I3, I4$ are the following integrals:

$$I1 = \int_0^d \sinh(\alpha_{km}^{(1)} y) \cdot (\sinh(\alpha_{kn}^{(1)} y))^* \, dy$$

$$I2 = \int_0^d \cosh(\alpha_{km}^{(1)} y) \cdot (\cosh(\alpha_{kn}^{(1)} y))^* \, dy$$

$$I3 = \int_d^h \sinh(\alpha_{km}^{(2)}(h-y)) \cdot (\sinh(\alpha_{km}^{(2)}(h-y)))^* \, dy$$

$$I4 = \int_d^h \cosh(\alpha_{km}^{(2)}(h-y)) \cdot (\cosh(\alpha_{km}^{(2)}(h-y)))^* \, dy.$$

REFERENCES

[1] R. K. Hoffman, *Integrierte Mikrowellenshcaltungen*. Berlin: Springer-Verlag, 1983.

[2] K. C. Gupta, R. Garg, and I. J. Bahl, *Microstrip Lines and Slotlines*. Dedham, MA: Artech House, 1979, sec. 3.4.3.

[3] K. C. Gupta, R. Garg, and R. Chadha, *Computer Aided Design of Microwave Circuits*. Dedham, MA: Artech House, 1981, sec 6 2.4

[4] T. C. Edwards, *Foundations for Microstrip Circuit Design*. New York: Wiley, 1981, secs. 5.8, 5.13.
[5] R. Mehran, *Grundelemente des rechnergestützten Entwurfs von Mikrostreifenleitungs — Schaltungen*. Aachen: Verlag H. Wolff, 1983.
[6] N. H. L. Koster and R. H. Jansen, "The microstrip step discontinuity: A revised description," *IEEE Trans. Microwave Theory Tech.*, vol. MTT-34, pp. 213–222, 1986.
[7] P. Benedek and P. Silvester, "Equivalent capacitances for microstrip gaps and steps," *IEEE Trans. Microwave Theory Tech.*, vol. MTT-20, pp. 729–733, 1972.
[8] A. F. Thomson and A. Gopinath, "Calculation of microstrip discontinuity inductances," *IEEE Trans. Microwave Theory Tech.*, vol. MTT-23, pp. 648–654, 1975.
[9] I. Wolff, G. Kompa, and R. Mehran, "Calculation method for microstrip discontinuities and T junctions," *IEEE Electron. Lett.*, vol. 8, pp. 177–179, 1972.
[10] G. Kompa, "Design of stepped microstrip components," *Radio Electron. Eng.*, vol. 48, pp. 53–63, 1978.
[11] R. H. Jansen, "Hybrid mode analysis of end effects of planar microwave and millimeterwave transmission lines," *Proc. Inst. Elec. Eng.*, vol. 128, pt. H., pp. 77–86, 1981.
[12] R. H. Jansen, "The spectral-domain approach for microwave integrated circuits," *IEEE Trans. Microwave Theory Tech.*, vol. MTT-33, pp. 1043–1056, 1985.
[13] R. Mittra and T. Itoh, "A new technique for the analysis of the dispersion characteristics of microstrip lines," *IEEE Trans. Microwave Theory Tech.*, vol. MTT-19, pp. 47–56, 1971.
[14] T. S. Chu, T. Itoh, and Yi-Chi Shih, "Comparative study of mode matching formulations for microstrip discontinuity problems," *IEEE Trans. Microwave Theory Tech.*, vol. MTT-33, pp. 1018–1023, 1985.
[15] L. P. Schmidt, "Rigorous computation of the frequency dependent properties of filters and coupled resonators composed from transverse microstrip discontinuities," in *Proc. 10th European Microwave Conf.* (Warsaw, Poland), 1980, pp. 436–440.
[16] W. L. Chang, "Filterelemente und Resonatoren aus geschirmten streifenleitungen mit sprunghafter, Breitenänderung," Ph.D. thesis, TH Darmstad, W. Germany, 1977.
[17] R. Mittra and T. Itoh, "Analysis of Microstrip Transmission Lines," in *Advances in Microwaves*, vol. 8, L. Young and H. Sobol, Eds. New York: Academic Press, 1974, pp. 121–122.
[18] P. Daly, "Hybrid-mode analysis of microstrip by finite element methods," *IEEE Trans. Microwave Theory Tech.*, vol. MTT-19, pp. 19–25, 1971.
[19] A. S. Omar and K. Schünemann, "Formulation of the singular integral equation technique for planar transmission lines," *IEEE Trans. Microwave Theory Tech.*, vol. MTT-33, pp. 1313–1321, 1985.
[20] R. Mittra and S. W. Lee, *Analytical Techniques in the Theory of Guided Waves*. New York: Macmillan, 1971.

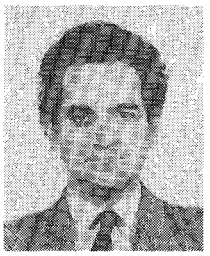

Nikolaos K. Uzunoglu (M'82) received the B.Sc. degree in electronics engineering from the Istanbul Technical University, Turkey, in 1973. He obtained the M.Sc. and Ph.D. degrees from the University of Essex, England, in 1974 and 1976, respectively.

He worked for the Hellenic Navy Research and Technology Development Office from 1977 to 1984. During this period, he also worked on a part-time basis at the National Technical University on electromagnetic theory. In 1984, he was elected Associate Professor at the National Technical Institute University of Athens, the position that he holds presently. His research interests are microwave applications, fiber optics, and electromagnetic theory.

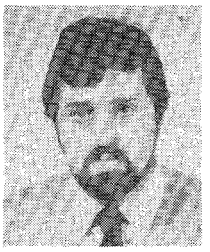

Christos N. Capsalis was born in Nafplion, Greece, on September 25, 1956. He received the Diploma of E.E. and M.E. from the National Technical University of Athens (NTUA), Greece, in 1979 and the bachelor's degree in economics from the University of Athens, Greece, in 1983. He also received the Ph.D. degree in electrical engineering from NTUA in 1985.

Since January 1982, he has been a Research Associate in the Department of Electrical Engineering at NTUA. In November 1986 he was elected Lecturer at NTUA, the position that he currently holds. His main research interests are in the electromagnetic field area, with emphasis on scattering and propagation at millimeter and optical wavelengths.

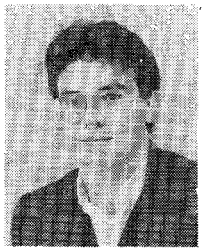

Constantinos P. Chronopoulos was born in Tripolis, Greece, in 1964. He received the Diploma in electrical engineering from the National Technical University of Athens (NTUA) in 1986. Since then, he has been working at NTUA toward the Ph.D. degree with a scholarship from the Bodosakis Foundation. His thesis deals with microstrip discontinuities. His main field of interest includes fiber optics and millimeter-wave applications.